

Eccentric Signatures of Stellar-Mass Binary Black Holes with Circumbinary Disks in LISA

Isobel M. Romero-Shaw^{1,2*}, Samir Goorachurn^{3,4}, Magdalena Siwek⁵, and Christopher J. Moore^{6,1,2}

¹ *Department of Applied Mathematics and Theoretical Physics, Cambridge CB3 0WA, United Kingdom*

² *Kavli Institute for Cosmology Cambridge, Madingley Road Cambridge CB3 0HA, United Kingdom*

³ *Physics and Astronomy Department Galileo Galilei, University of Padova, Via Marzolo, 8-35131, Padova, Italy*

⁴ *Department of Physics, McGill University, 3600 University Street, Montréal, QC H3A 2T8, Canada*

⁵ *Center for Astrophysics, Harvard University, Cambridge, MA 02138, USA*

⁶ *Institute of Astronomy, University of Cambridge, Cambridge, CB3 0HA, United Kingdom*

Accepted XXX. Received YYY; in original form ZZZ

ABSTRACT

Stellar-mass binary black holes may have circumbinary disks if formed through common-envelope evolution or within gaseous environments. Disks can drive binaries into wider and more eccentric orbits, while gravitational waves harden and circularise them. We combine cutting-edge evolution prescriptions for disk-driven binaries with well-known equations for gravitational-wave-driven evolution, and study the evolution of stellar-mass binary black holes. We find that binaries are driven by their disk to an equilibrium eccentricity, $0.2 \lesssim e_{\text{eq}} \lesssim 0.5$, that dominates their evolution. Once they transition to the GW-dominated regime their eccentricity decreases rapidly; we find that stellar-mass binary black holes with long-lived disks will likely be observed in LISA with detectable eccentricities $\sim 10^{-2}$ at 0.01 Hz, with the precise value closely correlating with the binary’s initial mass ratio. This may lead stellar-mass binary black holes with CBDs observed in LISA to be confused with dynamically-formed binary black holes.

Key words: gravitational waves – stars: black holes – transients: black holes mergers

1 INTRODUCTION

Binary black holes (BBHs) evolving within circumbinary disks (CBDs) can be driven to long-lasting equilibrium eccentricities (D’Orazio & Duffell 2021; Zrake et al. 2021; Siwek et al. 2023b). Merging stellar-mass BBHs form via several pathways that may involve CBDs: for example, an isolated binary may go through common envelope (CE) evolution (Paczynski 1976; Livio & Soker 1988; Bethe & Brown 1998; Dominik et al. 2012; Ivanova et al. 2013; Kruckow et al. 2016; Stevenson et al. 2017), while a dynamically-assembled binary may evolve while embedded in an active galactic nuclei (AGN) disk (Bartos et al. 2017; McKernan et al. 2018; Yang et al. 2019; McKernan et al. 2020; Gröbner et al. 2020; Ford & McKernan 2022; Samsing et al. 2022; Calcino et al. 2023), and binaries evolving in field triples may also gain CBDs (Silsbee & Tremaine 2017; Antonini et al. 2017a; Liu & Lai 2017; Liu et al. 2019; Vigna-Gómez et al. 2021; Dorozsmai et al. 2024). Dynamical assembly in dense star clusters is not thought to produce BBHs with CBDs, since frequent BH partner-swappings and interactions likely disrupt disk formation (Wen 2003; Askar et al. 2017; Rodriguez et al. 2018a,b; Samsing 2018; Antonini & Rasio 2016; Hoang et al. 2018; Fragione & Bromberg 2019; Chattopadhyay et al. 2023). Identifying the influence of a CBD on the orbit of a BBH can therefore distinguish between different formation environments.

For BBHs detected with the current generation of ground-based detectors, measurable eccentricity is considered a robust indicator of dynamical formation (Lower et al. 2018; Zevin et al. 2021). Isolated BBHs are expected to have negligible eccentricities in ground-based detectors, but close-to-merger eccentricities in dynamically-formed or tertiary-driven BBH can be higher, with different pathways yielding distinct eccentricity distributions (e.g., Samsing 2018; Antonini et al. 2017b; Rodriguez et al. 2018a; Tagawa et al. 2021; Arca Sedda et al. 2021; Samsing et al. 2022). For example, BBHs forming in globular clusters (GCs) have $10^{-8} \lesssim e_{10} \lesssim 10^{-3}$ if ejected from the cluster, $10^{-7} \lesssim e_{10} \lesssim 10^{-2}$ if they merge between dynamical interactions, and $10^{-3} \lesssim e_{10} \lesssim 1$ if they merge through GW capture (Zevin et al. 2021). The limited eccentricity sensitivity of Advanced LIGO-Virgo-KAGRA (LVK) (Abbott et al. 2018) detectors permits a narrow window onto eccentricity distributions: we are sensitive to only $e_{10} \gtrsim 0.05$ at GW frequencies of 10 Hz (Lower et al. 2018). Just a small fraction of the multi-peaked distribution predicted for BBHs in GCs, which differs from those arising in other environments like AGN disks and field triples, can be used to distinguish a population of GC mergers from other channels in current detectors (Romero-Shaw et al. 2022).

Future space-based detector LISA (Amaro-Seoane et al. 2022) will unlock a lower-frequency stretch of the GW spectrum: $10^{-4} \lesssim f_{\text{GW}} \lesssim 0.1$ Hz. LISA will be most sensitive to chirping stellar-mass BBHs approximately 10 years before they merge, at frequencies ~ 0.01 Hz (Gerosa et al. 2019). While LISA’s observable volume for

* E-mail: ir346@cam.ac.uk

chirping stellar-mass BBHs is small, we do expect to capture several tens of inspiralling systems within redshifts $z \lesssim 0.1$ (Gerosa et al. 2019; Wang et al. 2021; Klein et al. 2022). Within the Milky Way, LISA may see ~ 5 BBHs at lower frequencies, $\approx 10^{-4} - 10^{-3}$ Hz, where their slow evolution will give them quasi-monochromatic GW emission (Strokov & Berti 2024); a key challenge will be distinguishing more exotic sources like this from the dominant white dwarf binary background (Moore et al. 2023).

Since GW frequency increases as the binary separation shrinks, LISA will observe earlier stages of a stellar-mass BBH’s life compared to ground-based detectors. Since GWs circularise orbits, younger systems are also likely to have higher eccentricities (Peters 1964). With LISA sensitivity, eccentricities $\gtrsim 10^{-3}$ can be measured for stellar-mass BBHs inspiralling through the LISA band at a GW frequency of 0.01 Hz (Klein et al. 2022; Garg et al. 2023; Wang et al. 2024). Binaries evolving in isolation are expected to have $10^{-5} \lesssim e_{0.01} \lesssim 10^{-3}$ at 0.01 Hz, those merging after ejection from their host cluster have $10^{-4} \lesssim e_{0.01} \lesssim 10^{-2}$, and in-cluster mergers will have $e_{0.01} \gtrsim 10^{-2}$ (Wang et al. 2024). Eccentricity is therefore likely to be a common feature of stellar-mass BBHs in LISA.

Interactions of a BBH with a CBD can cause distinct observables, which may facilitate the identification of CBD-driven BBH mergers. Such observables include electromagnetic counterparts (e.g., Mösta et al. 2010; Martin et al. 2018), and mass ratios closer to unity due to preferential accretion onto the less massive component (e.g., Farris et al. 2014; Gerosa et al. 2015; Duffell et al. 2020; Siwek et al. 2023a). As we show in this work, another feature that could distinguish stellar-mass BBHs with CBDs is distinct and measurable eccentricity values at 0.01 Hz, $e_{0.01} \sim 10^{-2}$. We find that the value of $e_{0.01}$ correlates with the binary’s initial mass ratio q_i , meaning that it may also correlate with the final mass ratio q_f if the BBH torques the CBD sufficiently to prevent accretion (Martin et al. 2018). Alternatively, a population of $q_f \approx 1$ BBHs may have their initial distribution of q_i mapped by their detected $e_{0.01}$.

Torques from a CBD can act to contrast or amplify the effects of GW emission. GW emission can *only* remove energy from a binary, thereby always reducing its separation and eccentricity (Peters 1964). Analytical and early numerical simulations (e.g., Pringle 1991; Gould & Rix 2000; Armitage & Natarajan 2002; Haiman et al. 2009) showed that the presence of a CBD would also facilitate inspiral. More recent hydrodynamic simulations, however, which resolve the gas dynamics *within* the central cavity of the CBD, show that CBDs can cause binary inspiral *or* outspiral, (e.g., Miranda et al. 2016; Muñoz et al. 2019; D’Orazio & Duffell 2021) depending on many factors (e.g., disk thickness (Tiede et al. 2020), viscosity (Heath & Nixon 2020), binary mass ratio and eccentricity (Siwek et al. 2023b)), if the disk mass is comparable to the mass of the binary (Valli et al. 2024). Hydrodynamical simulations also show that resonant disk-binary interactions typically increase the eccentricity of binaries that start close to circular (Goldreich & Tremaine 1979). The eccentricity saturates at a limiting value (Lubow & Artymowicz 1992; Zrake et al. 2021; D’Orazio & Duffell 2021), the “equilibrium eccentricity” e_{eq} , that depends on the binary mass ratio (Siwek et al. 2023b), if the mass of the CBD is at least a few percent of the binary’s mass (Valli et al. 2024).

Ishibashi & Gröbner (2020) developed an analytic model to combine the driving factors of gas torques and GW emission on BBH embedded in AGN disks, with disk properties dependent on the mass and proximity of the central supermassive BH. They estimate the eccentricities of equal-mass BBH with $M = 50 M_{\odot}$ in LISA to be in the range 0.01–0.1. Ishibashi & Gröbner (2024) updated the simplified analytic model to include the effects of accretion, studying three dif-

ferent total masses and five different mass ratios. Zrake et al. (2021) combine hydrodynamical simulations with equations for GW-driven evolution from Peters (1964) to evolve equal-mass BBHs of masses ranging from stellar to supermassive, finding all equal-mass BBHs have $e_{\text{eq}} \sim 0.45$ as a result of gas driving, and that an $M = 147 M_{\odot}$ binary at redshift $z = 1$ has $e \sim 5 \times 10^{-3}$ at ~ 0.01 Hz. For other classes of LISA sources, such as the much heavier and louder supermassive BBH mergers, eccentricities can be measured at lower frequencies; for example, Armitage & Natarajan (2005); Roedig et al. (2011); Siwek et al. (2024) all predict that $10^6 M_{\odot}$ BBHs retain $e \gtrsim 10^{-3}$ in LISA.

Here, we combine cutting-edge detailed hydrodynamical simulations of BBHs with CBD (Siwek et al. 2023b) with the formulae of Peters (1964) for the evolution of orbital parameters under GW emission. We study a range of binary total masses $M \in (33, 60) M_{\odot}$ and initial eccentricities $e_i \in (0, 0.8)$, finding that these binaries have equilibrium eccentricities between $0.2 \lesssim e_{\text{eq}} \lesssim 0.5$, depending on initial mass ratio. As they evolve to higher frequencies and smaller separations, GW-driven evolution takes over, and the eccentricity begins to decay rapidly. The earlier CBD-driven evolution leaves its mark on the binary, leading to eccentricities $e_{0.01} \sim 10^{-2}$ at 0.01 Hz.

In Sec. 2, we describe our procedure for evolving stellar-mass BBH with CBDs; in Sec. 3, we report our results; and in Sec. 4, we summarise the implications of these results and discuss follow-up studies.

2 METHOD

The gas-driven evolution of BBHs is encapsulated by incremental changes in semi-major axis, \dot{a}_{gas} , and eccentricity, \dot{e}_{gas} . Rates of change are derived in Siwek et al. (2023b) for systems with different initial mass ratios, q_i , and initial eccentricities, e_i . The evolution rates are scaled by the initial separation, a_i , and initial total mass of the binary, M_i . We use the orbital evolution prescriptions published in Siwek et al. (2023b), computed using a grid of hydrodynamical simulations created using the Navier Stokes version of moving-mesh code Arepo (Springel 2010; Pakmor et al. 2016). The disk viscosity, $\nu = \alpha(h/r)^2 r^2 \sqrt{GM/r^3}$, is parameterized by a constant $\alpha = 0.1$ (Shakura & Sunyaev 1973), and the disk aspect ratio is fixed at $h/r = 0.1$. The results of these simulations are in good agreement with the results of simulations using other codes that employ similar methods, e.g., Muñoz et al. (2019); D’Orazio & Duffell (2021); Zrake et al. (2021).

The evolution rates calculated in Siwek et al. (2023b) are valid for generic binary-plus-disk systems. Their scaling to physical quantities, e.g., the absolute accretion rate and electromagnetic luminosity, depends on the ratio of accretion efficiency in Eddington units, f_e , to the radiative efficiency parameter ϵ . The latter may take a value between 0 and 1, and represents the fraction of the rest mass energy of the object lost as radiation during the accretion process. The gravitational potential energy of a particle in the disk can be lost due to friction-induced gas heating. For single BHs, ϵ ranges between about 0.06 for Schwarzschild BHs and 0.32 for maximally-spinning BHs (Laor & Netzer 1989). Interactions of BHs with each other and with their circumbinary disk, as well as poorly-constrained mechanisms of radiative feedback, make ϵ uncertain for BBH evolution. We use a conservative estimate of $\epsilon = 0.1$. We note that $f_e/\epsilon = 0.1$ (when $f_e = 0.01$, $\epsilon = 0.1$) could equally be achieved with, for example, $f_e = 0.1$, $\epsilon = 1$.

Each simulated grid of BBHs comprises 90 systems with ten initial mass ratios uniformly distributed in the range $0.1 \leq q_i \leq 1.0$ and

nine initial eccentricities uniformly distributed in the range $0.0 \leq e_i \leq 0.8$, matching the grid of parameters covered in Siwek et al. (2023b). We evolve these binaries over a grid of ten f_e values in the range $0.01 \leq f_e \leq 0.1$. Our main results are shown for binaries of initial primary mass $m_{1,i} = 30 M_\odot$. Our lowest initial secondary mass is therefore $3 M_\odot$, a rather low BH mass that can arise through CE evolution (Zevin et al. 2020) if the instability growth timescale in supernovae is assumed to be ~ 200 ms (the ‘‘Delayed’’ prescription of Fryer et al. 2012). We also run otherwise-identical simulations with initial total mass $M_i = 60 M_\odot$.

We initialise each binary with a small semi-major axis of 0.2 au to probe the regime where GWs may compete with the CBD, since GW emission only starts to influence the evolution significantly at separations on this scale. This is also a reasonable distance to initiate BBHs immediately post-CE; indeed, separations immediately following CE can be much smaller (e.g., Stevenson et al. 2017; Belczynski 2020). We compare results with and without including the effects of accretion; details of the implementation are given in Section 2.1.

The GW-driven evolution of binary black holes is described by the equations of Peters (1964):

$$\dot{a}_{\text{GW}} = \frac{-64}{5} \left(\frac{G^3 M^3}{c^5 a^3 (1-e^2)^{7/2}} \right) \left(1 + \frac{73}{24} e^2 + \frac{37}{96} e^4 \right), \quad (1)$$

$$\dot{e}_{\text{GW}} = \frac{-304}{15} e \left(\frac{G^3 M^3}{c^5 a^4 (1-e^2)^{5/2}} \right) \left(1 + \frac{121}{304} e^2 \right), \quad (2)$$

where \dot{a}_{GW} and \dot{e}_{GW} are the evolution rates of the semi-major axis a and eccentricity e due to GW emission, G is the gravitational constant, c is the speed of light, and the chirp mass $M = (m_1 m_2)^{3/5} / (m_1 + m_2)^{1/5}$.

To calculate the combined effects of gas and GWs on the binary evolution, we calculate at each timestep the net change in a and e ,

$$\dot{a}_{\text{net}} = \dot{a}_{\text{gas}} + \dot{a}_{\text{GW}}, \quad \dot{e}_{\text{net}} = \dot{e}_{\text{gas}} + \dot{e}_{\text{GW}}. \quad (3)$$

We estimate f_{GW} as simply double the Keplerian orbital frequency of a circular binary with separation a , which corresponds to the frequency of the dominant harmonic for moderately-eccentric binaries.

2.1 Accretion of gas

While f_e represents the fraction of the Eddington accretion rate that a single BH of mass $M = m_1 + m_2$ would accrete at, the individual BHs likely accrete asymmetrically at different rates (Siwek et al. 2023a). This parameter can be considered a proxy for the surface density of the disk, providing a measure of how much gas is available to torque the binary: the denser the disk, the stronger the torque on the binary from the gas parcels that are distributed in the disk. The actual efficiency of mass accretion onto stellar-mass BBH from disks formed in post-CE systems is influenced by multiple uncertain factors, e.g., magnetic fields in gas disks of this type, which affect the rate of viscous transport.

We consider three accretion paradigms in this work. The first is *unlimited accretion*, representing a binary in an infinite gas reservoir that continually accretes mass. The second is *no accretion* (‘‘none’’ in Fig. 2), representing a binary in an infinite gas disk that continually interacts with the disk but does not accrete any matter at all. Negligible accretion may be the norm for post-CE BBHs with disks: ‘‘typical’’ binary-disk parameters for post-CE stellar-mass BBH are found to converge towards the zero-accretion case due to the torques

that the binary exerts on the disk (Martin et al. 2018). The third case is *limited accretion*, in which the disk mass is 10% of M_i , and the binary accretes until the disk runs out.

If the CBD contains less mass than the binary itself, accretion will deplete the disk before it has time to significantly influence its separation, although the steady-state eccentricity can be reached if the disk contains only 10% of the binary’s mass (Valli et al. 2024). If the binary components accrete, the mass and mass ratio of the binary are time-dependent and alter the eccentricity evolution. Mass accretion proceeds asymmetrically for unequal-mass binaries, with preferential accretion onto the lower-mass object; we implement this by interpolating the grid of $\lambda(q, e)$ values presented in Fig. 4 of Siwek et al. (2023a). In our limited accretion model, the disk mass $M_d = 0.1M$ and the system reverts to GW-only evolution once this is depleted. The influence of the disk likely decreases gradually as it loses mass to the binary and its surface density is reduced. We approximate this behaviour by multiplying \dot{a}_{gas} and \dot{e}_{gas} by the fraction of the disk mass remaining at that timestep, $1 - \delta M / M_d$. In our unlimited-accretion model, the binary accretes at f_e times its time-evolving Eddington limit throughout its evolution.

3 RESULTS

We compare examples of CBD-plus-GW-driven evolution to GW-only in Fig. 1 for initial eccentricities $e_i = 0.1, 0.8$, initial mass ratios $q_i = 0.1, 0.5, 1.0$, and a range of f_e . Consistent with Siwek et al. (2023b), we find that a binary is driven by its CBD towards an eccentricity that remains near-constant for a large fraction of its lifetime. For stellar-mass BBHs with CBDs, the equilibrium eccentricity e_{eq} generally persists for $O(\text{Gyr})$.

The CBD heavily influences the BBH merger timescale. While the GW-only merger timescale is a strong function of e_i , the GW-plus-gas timescale varies less with e_i and more with q_i . As the regulating influence of the disk is strongest when $f_e = 0.1$, in this case there is almost no difference in the merger timescales of binaries with the same q_i and but different e_i . For low q_i , the merger timescales are almost identical regardless of f_e .

As reported in Tab. 1, e_{eq} is set by q_i for all initial eccentricities $e_i > e_{i,\text{min}}$. The values we find are consistent with those reported in Valli et al. (2024). These eccentricities may not be observed in BBHs with $e_i \lesssim 0.05$, which rapidly circularise in all cases except equal-mass, and those with $f_e = 0.01$, $e_i \gtrsim 0.6$ and $q_i \approx 1$, which only briefly occupy the equilibrium eccentricity before recommencing their predominantly GW-driven decay (see the lower right panel of Fig. 1).

Stellar-mass BBHs with CBDs are candidates for multi-band observations and archival searches in LISA data. Fig. 2 shows the expected eccentricity at 0.01 Hz, $e_{0.01}$. We find $e_{0.01} \sim 10^{-2}$, within the range of detectability for such searches, and of the same magnitude as expected eccentricities from dynamically-formed mergers (Wang et al. 2024). The $e_{0.01}$ values remain set primarily by q_i , although for the unlimited-accretion case we expect $q_f \approx 1$. For the negligible-accretion case, in which $q_f = q_i$, this correlation a potential smoking-gun of BBHs with CBDs. We note that all $e_{0.01}$ values are given in the source frame, without considering the effects of the redshifting of the reference frequency. Using Peters (1964), we estimate that an eccentricity of $e = 3 \times 10^{-2}$ at 0.01 Hz is redshifted to $e = 2 \times 10^{-2}$ if $z = 0.2$ (10^{-3} if $z = 1$); see also Sec. 4.1.1 of Romero-Shaw et al. (2022). Redshifting therefore likely accounts for the much lower predicted $e_{0.01} \sim 2 \times 10^{-3}$ for the $q_i = 1$ BBH with $M_i = 147 M_\odot$ highlighted in Zrake et al. (2021), al-

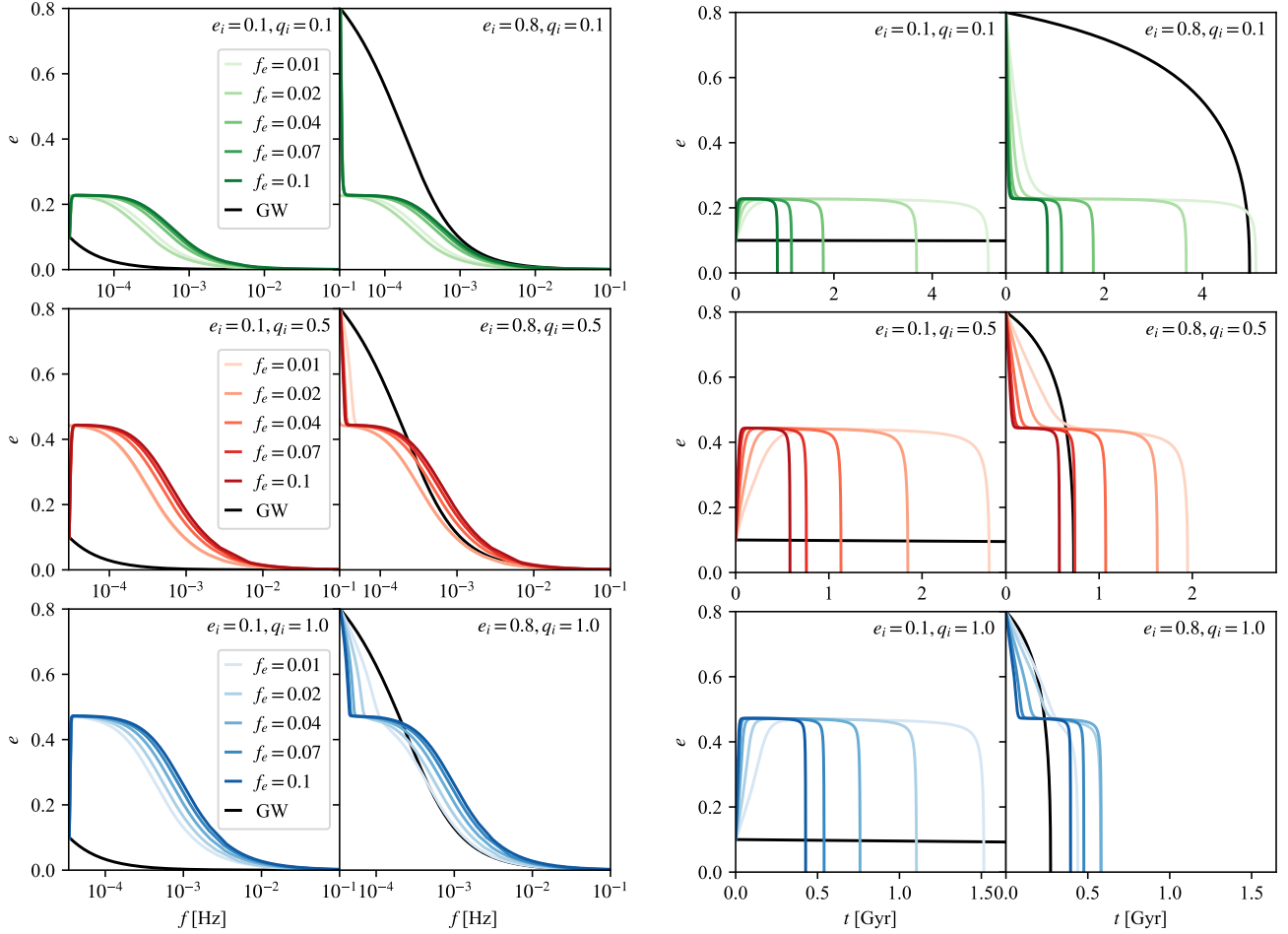


Figure 1. The eccentricity evolution of BBHs with $e_i = 0.1, 0.8$ (left and right columns, respectively, of each set of plots) and $q_i = 0.1, 0.5, 1.0$ (top to bottom rows) with initial $m_{1,i} = 30 M_\odot$, assuming *unlimited* accretion (see Sec. 2.1). The left set of plots shows the eccentricity evolution with peak GW frequency, while the right set of plots shows eccentricity evolution with time. The assumed f_e is indicated by the opacity of the curve. Because the CBD forces binaries with high e_i to smaller eccentricities much more rapidly than it shrinks their separation, these binaries evolve from higher to lower peak GW frequency before reaching their steady-state. The steady-state eccentricity decays above 10^{-4} Hz.

though higher-mass BBHs also circulate at lower frequencies than lower-mass BBHs.

The history of the binary is obscured by its interaction with the CBD. The worst concealment occurs for $q_i = 1$, where $e_{\text{eq}} \approx 0.47$ for $e_i > 0$ and $e_{\text{eq}} \approx 0.4$ for $e_i = 0$; further, we find that $e_{0.01} \approx 10^{-2}$ for all e_i . Equilibrium eccentricities found in D’Orazio & Duffell (2021); Zrake et al. (2021) for $q_i = 1$ are also $e_{\text{eq}} \approx 0.47$, although these studies see $q_i = 1, e_i \approx 0$ further circularise. Our results are consistent with those of Siwek et al. (2023b), so we chalk this up to the use of different hydrodynamical simulations rather than the inclusion of GW emission. In the final column Tab. 1, we show e_{eq} for BBHs with $M_i = 60 M_\odot$. Higher-mass systems reach slightly lower steady-state eccentricities; see also Zrake et al. (2021); Siwek et al. (2024).

All of our simulated binaries inspiral and merge, in contrast with previous studies (e.g., D’Orazio & Duffell 2021; Siwek et al. 2023b; Valli et al. 2024), which found expanding orbits for some $e_i = 0$ or low mass ratio binaries. This is a consequence of including GW emission: in areas of the e_i, q_i plane where \dot{a}_{gas} is positive in Fig. 1 of Valli et al. (2024), \dot{a}_{GW} is negative and much higher in magnitude. Taking $e_i = 0.4, q_i = 0.1, f_e = 0.1$ as an example, \dot{a}_{GW} is negative

and $\sim 10^7$ times higher in magnitude than \dot{a}_{gas} at $a = 0.2$ au, driving the binary quickly to smaller separations. At around $a = 0.1$ au, the sign of \dot{a}_{gas} also becomes negative; however, by now the GW emission dominates even more, and $\dot{a}_{\text{GW}}/\dot{a}_{\text{gas}} \sim 10^{14}$. The rapidity of eccentricity evolution for BBHs with CBDs is also explained by inspecting \dot{e}_{gas} and \dot{e}_{GW} ; for the same example system, both are negative, but $\dot{e}_{\text{gas}}/\dot{e}_{\text{GW}} \sim 6000$ at $a = 0.2$ au. This ratio becomes ~ 1 around $a = 0.1998$ au.

The GW frequency range within which a binary inhabits e_{eq} depends on f_e for two reasons. Firstly, since f_e represents the availability of gas that can torque the binary, a high f_e causes the binary evolution to be more strongly disk-driven and for longer. Secondly, if we allow $m_1, m_2 \geq 0$, the binary evolves more rapidly; in this case the mass in the disk can also be depleted rapidly, so the disk-driven epoch may be much shorter than the negligible-accretion case. The negligible-accretion case with $f_e = 0.1$ produces the highest-frequency transitions into the GW-dominated regime, leading to slightly higher eccentricities at 0.01 Hz, as shown in Fig. 2.

By the time the f_{GW} reaches 11 Hz, the optimistic minimum frequency of the future ground-based detector Einstein Telescope (ET; Maggiore et al. 2020), BBHs with CBDs have eccentricities

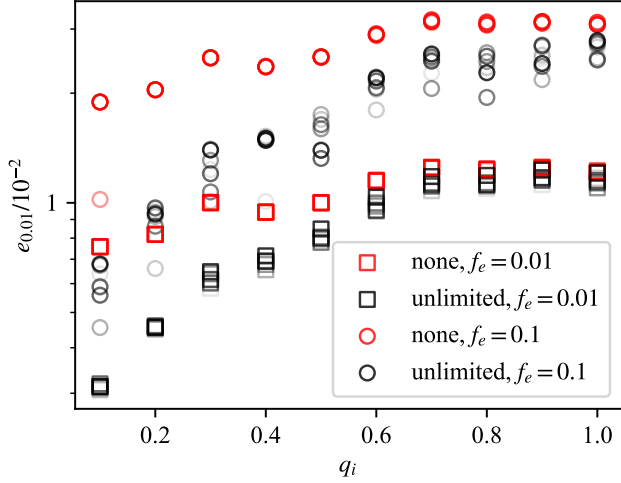


Figure 2. Eccentricities at 0.01 Hz for all binaries with $e_i > 0.05$. Square and circular scatter points correspond to $f_e = 0.01$ and 0.1 respectively. Colours correspond to the cases of *unlimited accretion* and *no accretion* ("none", red markers), both with long-lived disks; binaries without disks have $e_{0.01} < 10^{-3}$. The initial eccentricity corresponds to the alpha value of the scatter marker (higher e_i , higher opacity). For the negligible accretion case, e_i minimally affects $e_{0.01}$, while for unlimited accretion lower e_i can lead to slightly lower $e_{0.01}$. All values are detectable with LISA (Klein et al. 2022; Wang et al. 2024).

q_i	$e_{i,\min}$	$e_{\text{eq}}, m_{1,i} = 30 M_{\odot}$	$e_{\text{eq}}, M_i = 60 M_{\odot}$
0.1	0.10	0.224	0.224
0.2	0.05	0.298	0.297—0.298
0.3	0.05	0.302	0.301
0.4	0.05	0.401	0.401
0.5	0.05	0.437	0.437
0.6	0.05	0.489	0.488—0.489
0.7	0.05	0.504	0.503—0.504
0.8	0.05	0.470	0.470
0.9	0.05	0.470	0.470
1.0	0.00	0.469	0.469

Table 1. Value of the steady-state eccentricity reached in the CDB-dominated phase of the evolution for initial eccentricities above $e_{i,\min}$ when the binary has $a_i = 0.2$ au for varying initial mass ratios q_i . Below $e_{i,\min}$, the eccentricity reduces to $\lesssim 10^{-7}$. The values in this table are defined as the first eccentricity when $f_{\text{GW}} \geq 10^{-4}$ and $\dot{f}_{\text{GW}} \geq 0$. Our main results are presented for initial $m_{1,i} = 30 M_{\odot}$. The e_{eq} reached for initial total mass $M_i = 60 M_{\odot}$ is also shown in the rightmost column. There is slightly more variation for a higher M_i because higher-mass binaries have stronger GW emission than lower-mass binaries at the same GW frequency, so begin to become GW-dominated earlier. Where there is a range, higher values of e_{eq} occur for higher e_i .

$e_1 \approx 10^{-4}$ if $f_e = 0.1$, equivalent to $e_{10} \approx 10^{-5}$, below the expected sensitivity for ET (Lower et al. 2018; Saini 2024).

3.1 Accretion paradigms

Using the interpolated $\lambda(q, e)$ relationship from Siwek et al. (2023a) to split accreted mass unevenly between binary components, there is preferential accretion onto the lower-mass object, causing the binary to evolve towards $q_f = 1$. In Fig. 3, we compare the frequency- and time-domain eccentricity evolution of binaries with negligible,

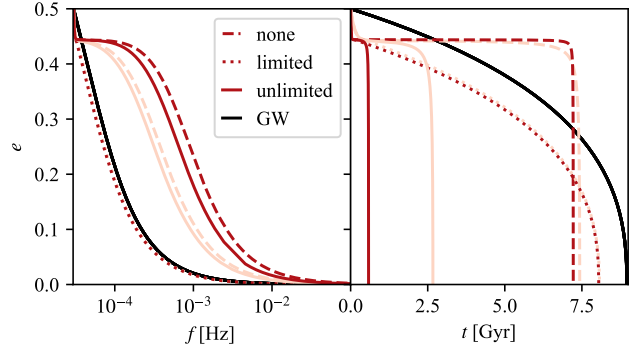


Figure 3. Frequency- (left) and time-domain (right) evolution of eccentricity for a binary with $q_i = 0.5$, $e_i = 0.5$ within different accretion paradigms. Darker and lighter colours indicate $f_e = 0.1$ and 0.01 , respectively, and the accretion assumption is indicated by the linestyle. Evolution with unlimited accretion is tracked with solid curves, while results using limited accretion have dotted curves, and those assuming no accretion have dashes.

limited and unlimited accretion for $q_i = 0.5$, $e_i = 0.5$. Like Ishibashi & Gröbner (2024), we find that unlimited accretion causes the binary to merge faster than if no accretion takes place, due to its increased mass and mass ratio. On the other hand, because a finite disk exists for long enough to push the binary to the equilibrium eccentricity but negligibly influences the separation (Valli et al. 2024), limited accretion leads to a longer circularisation and merger timescale.

3.1.1 Unlimited accretion

In reality, this scenario requires a plentiful gas reservoir that is long-lived and allows infinite accretion, like an AGN disk. We note that (a) AGN lifetimes may be much shorter than the Gyr timescales considered here and that (b) we are not considering the additional tidal force of an SMBH. When accretion is unlimited, binary masses equalise and the total binary mass grows substantially over its lifetime. Binaries finish their evolution with $q_f \approx 1$ and can multiply their total mass several times; the system illustrated in Fig. 3 goes from $M_i = 45 M_{\odot}$ to $M_f = 164$ (81) M_{\odot} and $q_f = 0.99$ (0.80) when $f_e = 0.1$ (0.01).

As the binary continues to accrete, its mass ratio tends towards unity, pushing the turnover to GW-driven evolution to slightly lower frequencies. Despite the mass increasing significantly during unlimited accretion, the evolution of eccentricity with frequency remains similar to the negligible-accretion case, but causes a softer transition to the GW-dominated regime. Because binaries with higher masses and mass ratios evolve faster, the accreting binary circularises and merges several Gyr earlier than the GW-only, negligible- or limited-accretion cases.

3.1.2 Limited accretion

The initial CBD mass, M_d , is set to 10% of the binary's total mass, an appropriate estimate for the mass contained in the CBD for post-CE systems (e.g., Heath & Nixon 2020; Valli et al. 2024). The evolution of $f_e = 0.1$ and $f_e = 0.01$ systems are very similar when the disk mass is limited because it is depleted within only ~ 0.04 Gyr, and the binary then evolves under the influence of GWs only. As shown in Fig. 3, the eccentricity evolution proceeds at slightly lower frequencies than the GW-only case because the disk causes eccentricity to be

driven down faster than separation. This binary merges ≈ 1 Gyr faster when it has a limited CBD because of this initial rapid circularisation. As in Valli et al. (2024), a depleting disk with $M_d = 0.1M_i$ exists for long enough to drive the BBH to the equilibrium eccentricity, but not to significantly influence its separation or mass ratio; in this example, the mass ratio grows by 0.06 and the mass grows by $\sim 4.5 M_\odot$.

4 DISCUSSION

The LISA-band eccentricity evolution of a stellar-mass BBH is markedly different when it has a CBD, as the CBD drives the binary to a characteristic equilibrium eccentricity determined by its initial mass ratio. We find that both e_{eq} and $e_{0.01}$ directly correspond to q_i , insensitively to assumptions about accretion efficiency. As long as the disk endures, the eccentricity at $f_{\text{GW}} = 0.01$ Hz is $e_{0.01} \sim 10^{-2}$, detectable for LISA and in the range usually expected for diskless dynamically-formed in-cluster mergers (Klein et al. 2022; Garg et al. 2023; Wang et al. 2024; DePorzio et al. 2024). Since $e_{0.01}$ is a strong function of q_i , a population of BBHs observed with an eccentricity-mass ratio correlation would indicate contributions from non-accreting BBHs with CBDs, while a population of $q = 1$ stellar-mass BBHs with eccentricities $e_{0.01} \sim 2 \times (10^{-3} - 10^{-2})$ would more likely come from accreting BBHs with CBDs. The values of $e_{0.01}$ that we predict for stellar-mass BBHs with CBDs are similar to those predicted for more massive BBHs with CBDs when they enter the LISA band (Armitage & Natarajan 2005; Roedig et al. 2011; Zrake et al. 2021; Siwek et al. 2024); across all mass scales, BBHs with CBDs may be characterised by distinct mass ratios and eccentricities in LISA, once redshifting is corrected for.

BBHs with CBDs are candidates for multi-band detections, and may be uncovered in LISA data through archival searches (Wang et al. 2024). CBDs may lead to eccentricities $\mathcal{O}(10^{-5})$ at 10 Hz in ET, higher than expected from isolated binaries but below the detectable threshold for GW150914-like BBHs (Lower et al. 2018). The detection threshold is likely lower for lower-mass binaries (Romero-Shaw et al. 2021), but a full population injection-recovery study is required to establish if any binaries with CBD-driven eccentricity could be identified with 3G detectors like ET.

The eccentricity evolution of stellar-mass BBHs with CBDs is similar to that of the supermassive BBHs evolved in Siwek et al. (2024), but proceeds at higher frequencies and slightly higher eccentricities due to the lower mass. Our results using limited accretion agree with those of Valli et al. (2024): disks with $M_d = 0.1M_i$ do not drastically influence the separation of the BBH, but do drive the binary eccentricity to its equilibrium value. The e_{eq} values we find for stellar-mass BBHs are in good agreement with the equilibrium eccentricity values found in Valli et al. (2024), with the maximum equilibrium eccentricity of $e_{\text{eq}} \approx 0.5$ occurring for $q_i = 0.7$. However, in contrast to previous work including Siwek et al. (2023b,a); Valli et al. (2024), none of our binaries undergoes orbital expansion, since $\dot{a}_{\text{GW}} \gg \dot{a}_{\text{gas}}$ when $a_i = 0.2$ au.

CBD-driven evolution obscures the history of the binary by driving it to higher or lower eccentricity than it started with, possibly causing very different evolution pathways (e.g., CE versus dynamical formation in an AGN disk) to produce BBHs with the same characteristic eccentricities and quasi-monochromatic appearance in LISA. CBDs can also induce large changes in merger time, leading to skewed rate estimates. However, the different expected distributions of M_i , q_i , and disk parameters for different formation channels could still lead to different population-level eccentricity distributions. Adjusting our simulation parameters to account for these differences will

be a crucial step in identifying BBHs with CBDs of alternate origin with LISA, and will be implemented in follow-up studies. Further work is also needed to predict e_{eq} and $e_{0.01}$ over an astrophysically-motivated M_i and q_i distributions for these stellar-mass BBHs, and to establish exactly how detectable these populations may be.

ACKNOWLEDGEMENTS

The authors are grateful to the organisers of the GWPAW 2022 conference in Melbourne, Australia, at which this work was initiated. We also thank Stan DeLaurentiis, Andris Doroszmaj, and Saavik Ford for useful discussions. IMR-S acknowledges support received from the Herchel Smith Postdoctoral Fellowship Fund. CJM acknowledges the support of the UK Space Agency grant, no. ST/V002813/1.

DATA AVAILABILITY

The data used to produce these results, namely the simulation outputs of Siwek et al. (2023b), are available upon reasonable requests made to MS. CBD-plus-GW binary evolution codes and outputs will also be made available upon request to IMR-S.

REFERENCES

- Abbott B. P., et al., 2018, *Living Rev. Rel.*, 21, 3
- Amaro-Seoane P., et al., 2022, *Astrophysics with the Laser Interferometer Space Antenna*, doi:10.48550/ARXIV.2203.06016, <https://arxiv.org/abs/2203.06016>
- Antonini F., Rasio F. A., 2016, *ApJ*, 831, 187
- Antonini F., Toonen S., Hamers A. S., 2017a, *Astrophys. J.*, 841, 77
- Antonini F., Toonen S., Hamers A. S., 2017b, *ApJ*, 841, 77
- Arca Sedda M., Li G., Kocsis B., 2021, *A&A*, 650, A189
- Armitage P. J., Natarajan P., 2002, *The Astrophysical Journal*, 567, L9
- Armitage P. J., Natarajan P., 2005, *ApJ*, 634, 921
- Askar A., Szkudlarek M., Gondek-Rosińska D., Giersz M., Bulik T., 2017, *MNRAS*, 464, L36
- Bartos I., Kocsis B., Haiman Z., Márka S., 2017, *ApJ*, 835, 165
- Belczynski K., 2020, *ApJ*, 905, L15
- Bethe H. A., Brown G. E., 1998, *Astrophys. J.*, 506, 780
- Calcino J., Dempsey A. M., Dittmann A. J., Li H., 2023, *arXiv e-prints*, p. arXiv:2311.13727
- Chattopadhyay D., Stegmann J., Antonini F., Barber J., Romero-Shaw I. M., 2023, *MNRAS*, 526, 4908
- D’Orazio D. J., Duffell P. C., 2021, *ApJ*, 914, L21
- DePorzio N., Randall L., Xianyu Z.-Z., 2024, *arXiv e-prints*, p. arXiv:2402.09513
- Dominik M., Belczynski K., Fryer C., Holz D. E., Berti E., Bulik T., Mandel I., O’Shaughnessy R., 2012, *ApJ*, 759, 52
- Doroszmaj A., Toonen S., Vigna-Gómez A., de Mink S. E., Kummer F., 2024, *MNRAS*, 527, 9782
- Duffell P. C., D’Orazio D., Derdzinski A., Haiman Z., MacFadyen A., Rosen A. L., Zrake J., 2020, *The Astrophysical Journal*, 901, 25
- Farris B. D., Duffell P., MacFadyen A. I., Haiman Z., 2014, *The Astrophysical Journal*, 783, 134
- Ford K. E. S., McKernan B., 2022, *MNRAS*, 517, 5827
- Fragione G., Bromberg O., 2019, *arXiv e-prints*, p. arXiv:1903.09659
- Fryer C. L., Belczynski K., Wiktorowicz G., Dominik M., Kalogera V., Holz D. E., 2012, *ApJ*, 749, 91
- Garg M., Tiwari S., Derdzinski A., Baker J., Marsat S., Mayer L., 2023, The minimum measurable eccentricity from gravitational waves of LISA massive black hole binaries (arXiv:2307.13367)
- Gerosa D., Veronesi B., Lodato G., Rosotti G., 2015, *MNRAS*, 451, 3941

- Gerosa D., Ma S., Wong K. W. K., Berti E., O’Shaughnessy R., Chen Y., Belczynski K., 2019, *Phys. Rev. D*, **99**, 103004
- Goldreich P., Tremaine S., 1979, *ApJ*, **233**, 857
- Gould A., Rix H.-W., 2000, *ApJ*, **532**, L29
- Gröbner M., Ishibashi W., Tiwari S., Haney M., Jetzer P., 2020, *A&A*, **638**, A119
- Haiman Z., Kocsis B., Menou K., 2009, *ApJ*, **700**, 1952
- Heath R. M., Nixon C. J., 2020, *A&A*, **641**, A64
- Hoang B.-M., Naoz S., Kocsis B., Rasio F. A., Dosopoulou F., 2018, *ApJ*, **856**, 140
- Ishibashi W., Gröbner M., 2020, *A&A*, **639**, A108
- Ishibashi W., Gröbner M., 2024, *Mon. Not. Roy. Astron. Soc.*, **529**, 883
- Ivanova N., et al., 2013, *A&ARv*, **21**, 59
- Klein A., et al., 2022, *arXiv e-prints*, p. [arXiv:2204.03423](https://arxiv.org/abs/2204.03423)
- Kruckow M. U., Tauris T. M., Langer N., Szécsi D., Marchant P., Podsiadlowski P., 2016, *Astron. Astrophys.*, **596**, A58
- Laor A., Netzer H., 1989, *Monthly Notices of the Royal Astronomical Society*, **238**, 897
- Liu B., Lai D., 2017, *ApJ*, **846**, L11
- Liu B., Lai D., Wang Y.-H., 2019, *The Astrophysical Journal*, **881**, 41
- Livio M., Soker N., 1988, *Astrophys. J.*, **329**, 764
- Lower M., et al., 2018, *Phys. Rev. D*, **98**
- Lubow S. H., Artymowicz P., 1992, in *Binaries as Tracers of Star Formation*. pp 145–154
- Maggiore M., et al., 2020, *jcrap*, **2020**, 050
- Martin R. G., Nixon C., Xie F.-G., King A., 2018, *MNRAS*, **480**, 4732
- McKernan B., et al., 2018, *ApJ*, **866**, 66
- McKernan B., Ford K. E. S., O’Shaughnessy R., Wysocki D., 2020, *MNRAS*, **494**, 1203
- Miranda R., Muñoz D. J., Lai D., 2016, *Monthly Notices of the Royal Astronomical Society*, **466**, 1170
- Moore C. J., Finch E., Klein A., Korol V., Pham N., Robins D., 2023, *arXiv e-prints*, p. [arXiv:2310.06568](https://arxiv.org/abs/2310.06568)
- Mösta P., Palenzuela C., Rezzolla L., Lehner L., Yoshida S., Pollney D., 2010, *Phys. Rev. D*, **81**, 064017
- Muñoz D. J., Miranda R., Lai D., 2019, *ApJ*, **871**, 84
- Paczynski B., 1976, *Common Envelope Binaries*
- Pakmor R., Springel V., Bauer A., Mocz P., Muñoz D. J., Ohlmann S. T., Schaal K., Zhu C., 2016, *MNRAS*, **455**, 1134
- Peters P. C., 1964, *Phys. Rev.*, **136**, B1224
- Pringle J. E., 1991, *MNRAS*, **248**, 754
- Rodríguez C. L., Amaro-Seoane P., Chatterjee S., Rasio F. A., 2018a, *Phys. Rev. Lett.*, **120**, 151101
- Rodríguez C. L., Amaro-Seoane P., Chatterjee S., Kremer K., Rasio F. A., Samsing J., Ye C. S., Zevin M., 2018b, *Phys. Rev.*, **D98**, 123005
- Roedig C., Dotti M., Sesana A., Cuadra J., Colpi M., 2011, *MNRAS*, **415**, 3033
- Romero-Shaw I., Lasky P. D., Thrane E., 2021, *ApJ*, **921**, L31
- Romero-Shaw I., Lasky P. D., Thrane E., 2022, *ApJ*, **940**, 171
- Saini P., 2024, *MNRAS*, **528**, 833
- Samsing J., 2018, *Phys. Rev. D*, **D97**, 103014
- Samsing J., et al., 2022, *Nature*, **603**, 237
- Shakura N. I., Sunyaev R. A., 1973, *A&A*, **24**, 337
- Silsbee K., Tremaine S., 2017, *Astrophys. J.*, **836**, 39
- Siwek M., Weinberger R., Muñoz D. J., Hernquist L., 2023a, *MNRAS*, **518**, 5059
- Siwek M., Weinberger R., Hernquist L., 2023b, *MNRAS*, **522**, 2707
- Siwek M., Kelley L. Z., Hernquist L., 2024, *arXiv e-prints*, p. [arXiv:2403.08871](https://arxiv.org/abs/2403.08871)
- Springel V., 2010, *MNRAS*, **401**, 791
- Stevenson S., Vigna-Gómez A., Mandel I., Barrett J. W., Neijssel C. J., Perkins D., de Mink S. E., 2017, *Nature Communications*, **8**, 14906
- Strokov V., Berti E., 2024, *Phys. Rev. D*, **109**, 104013
- Tagawa H., Kocsis B., Haiman Z., Bartos I., Omukai K., Samsing J., 2021, *ApJ*, **907**, L20
- Tiede C., Zrake J., MacFadyen A., Haiman Z., 2020, *The Astrophysical Journal*, **900**, 43
- Valli R., et al., 2024, *arXiv e-prints*, p. [arXiv:2401.17355](https://arxiv.org/abs/2401.17355)
- Vigna-Gómez A., Toonen S., Ramirez-Ruiz E., Leigh N. W. C., Riley J., Haster C.-J., 2021, *ApJ*, **907**, L19
- Wang H., Stephan A. P., Naoz S., Hoang B.-M., Breivik K., 2021, *ApJ*, **917**, 76
- Wang H., Harry I., Nitz A., Hu Y.-M., 2024, *Phys. Rev. D*, **109**, 063029
- Wen L., 2003, *Astrophys. J.*, **598**, 419
- Yang Y., Bartos I., Haiman Z., Kocsis B., Márka Z., Stone N. C., Márka S., 2019, *ApJ*, **876**, 122
- Zevin M., Spera M., Berry C. P. L., Kalogera V., 2020, *ApJ*, **899**, L1
- Zevin M., Romero-Shaw I. M., Kremer K., Thrane E., Lasky P. D., 2021, *arXiv e-prints*, p. [arXiv:2106.09042](https://arxiv.org/abs/2106.09042)
- Zrake J., Tiede C., MacFadyen A., Haiman Z., 2021, *ApJ*, **909**, L13

This paper has been typeset from a \LaTeX file prepared by the author.